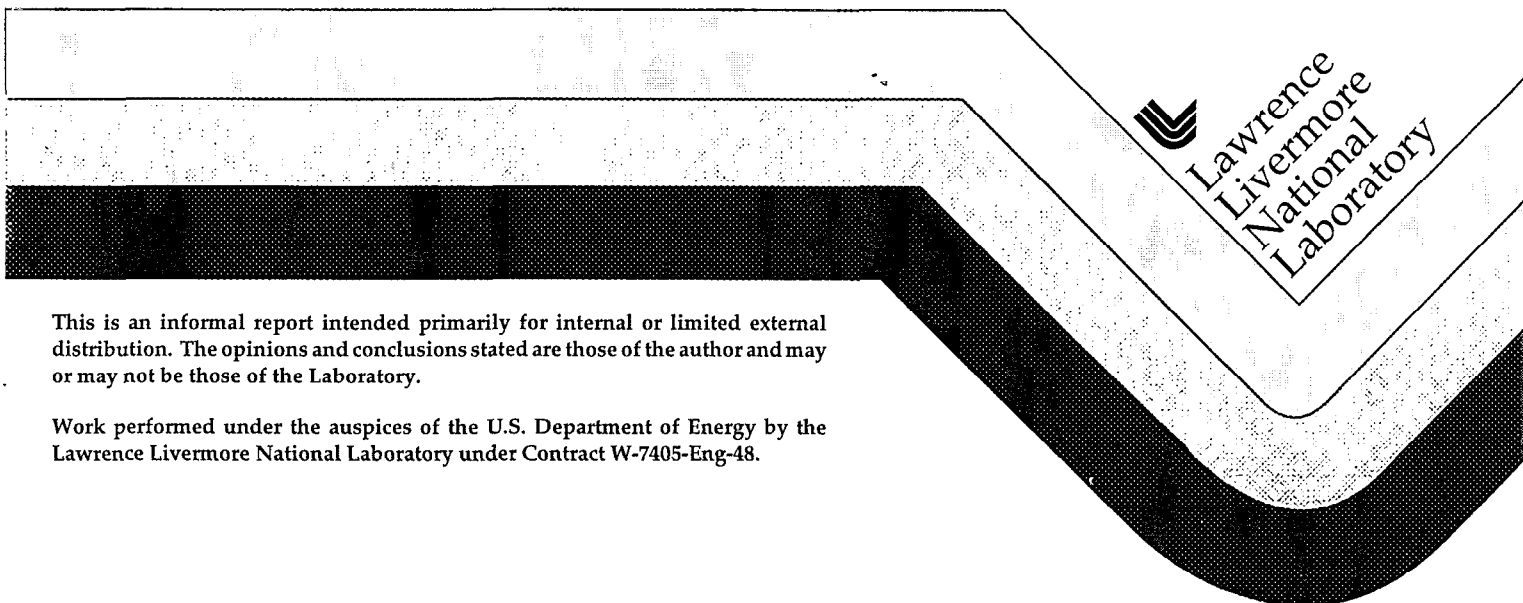


Laser Driven Radiography

M. D. Perry, J. Sefcik, T. Cowan, S. Hatchett,
M. Key, M. Moran, T. Phillips, D. Pennington,
R. Snavely, S. C. Wilks

December 20, 1997



This is an informal report intended primarily for internal or limited external distribution. The opinions and conclusions stated are those of the author and may or may not be those of the Laboratory.

Work performed under the auspices of the U.S. Department of Energy by the Lawrence Livermore National Laboratory under Contract W-7405-Eng-48.

DISCLAIMER

This document was prepared as an account of work sponsored by an agency of the United States Government. Neither the United States Government nor the University of California nor any of their employees, makes any warranty, express or implied, or assumes any legal liability or responsibility for the accuracy, completeness, or usefulness of any information, apparatus, product, or process disclosed, or represents that its use would not infringe privately owned rights. Reference herein to any specific commercial product, process, or service by trade name, trademark, manufacturer, or otherwise, does not necessarily constitute or imply its endorsement, recommendation, or favoring by the United States Government or the University of California. The views and opinions of authors expressed herein do not necessarily state or reflect those of the United States Government or the University of California, and shall not be used for advertising or product endorsement purposes.

This report has been reproduced
directly from the best available copy.

Available to DOE and DOE contractors from the
Office of Scientific and Technical Information
P.O. Box 62, Oak Ridge, TN 37831
Prices available from (615) 576-8401, FTS 626-8401

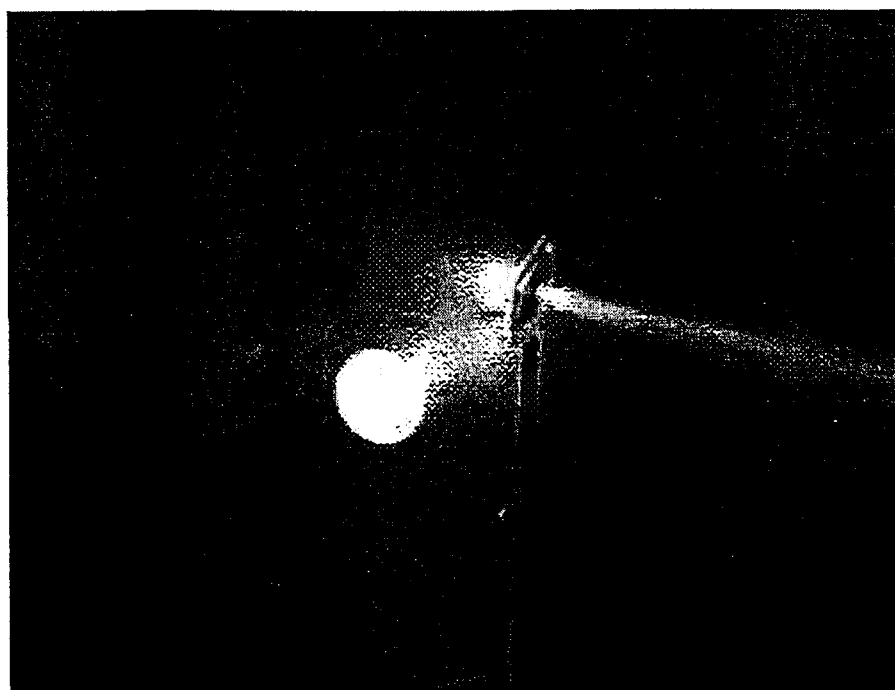
Available to the public from the
National Technical Information Service
U.S. Department of Commerce
5285 Port Royal Rd.,
Springfield, VA 22161

Laser Driven Radiography

14 April 1997
Revised 20 December 1997

M.D. Perry, J. Sefcik, T.Cowan, S. Hatchett, M. Key, M. Moran, T. Phillips,
D. Pennington, R. Snavely, and S.C. Wilks

*Lawrence Livermore National Laboratory, P.O. Box 808, L-439
Livermore, California 94550
phone (510) 423-4915*



Abstract

Intense laser ($>10^{21}$ W/cm²) driven hard x-ray sources offer a new alternative to conventional electron accelerator Bremsstrahlung sources. These laser driven sources offer considerable simplicity in design and potential cost advantage for multiple axis views. High spatial and temporal resolution is achievable as a result of the very small source size (<100 μ m) and short-duration of the laser pulse. We have begun a series of experiments with the Petawatt laser at LLNL to determine the photon flux achievable with these sources and assess their potential for Stewardship applications. Additionally, we are developing a conceptual design and cost estimate of a multi-pulse, multi-axis (up to five) radiographic facility utilizing the Contained Firing Facility at site 300 and existing laser hardware.

Laser Radiography Facility

Summary

A new source for high energy radiography for applications in high resolution, time resolved imaging in full scale hydrodynamic experiments is proposed. Preliminary calculations and experiments suggest that Petawatt class lasers can produce hard x-rays with a spectral distribution similar to that achievable with advanced high-current induction accelerators. Dose levels on the order of 100 Rads for photons >1 MeV should be achievable with multikilojoule, petawatt (1000 TW) laser pulses focused to an irradiance $\approx 10^{21}$ W/cm² onto a gold target. The advantages of these short-pulse laser produced x-ray sources for Stewardship applications are: 1) Multiple axis views are obtained simply by using mirrors to direct the pulses, 2) Extremely short pulse duration enables time gated detection, 3) Multiple pulse format is simple to achieve by producing multiple laser pulses, 4) Extremely small source size enables more sophisticated bremsstrahlung target designs and the possibility of higher spatial resolution, 5) Potential cost savings over accelerator technology, and 6) a laser based multiaxis system has numerous other applications when not being used for radiography (equation of state measurements, implosion physics and instability growth, x-ray drive, etc.)

The basic question regarding the viability of this source for radiography in Stockpile Stewardship applications is the achievable dose of high energy bremsstrahlung. The hard x-ray flux (photons/cm²-str) is produced by bremsstrahlung from relativistic currents in the target driven by the large electric field associated with the intense ($\approx 10^{21}$ W/cm²) short-pulse. Maximizing the photon flux on axis requires careful attention to the spatial and temporal quality of the laser pulse in order to achieve the maximum irradiance on the target. Preliminary results from the first Petawatt radiographic shot series (≈ 300 J on target) suggested that a dose of from 40-100 rads of hard (>1 MeV) photons may be achievable with 3-5 kJ, picosecond pulses. Further experiments and detailed calculations addressing these scaling arguments will be conducted throughout FY98.

The results of the highly successful September shot series are presented herein. In essence, they suggest that production of Stewardship relevant dose levels are limited by two technological issues: 1) production of a twice diffraction limited spot to achieve the necessary 10^{21} W/cm² on target and 2) scale-up of the size of dielectric gratings required to compress 5 kJ class pulses (to ≈ 80 cm from the current 15 cm).

In parallel to addressing the physics and technology questions associated with developing a radiographic facility based on Petawatt class lasers, we have also undertaken a conceptual design and cost estimate of a multi-axis radiographic facility based on the Contained Firing Facility at LLNL's site 300. The essential idea is to produce a pulse compressed 2x2 array of NIF laser beams. Each beam could produce two pulses up to 5 kJ in energy with an approximate pulse duration of 1 picosecond for a total of eight pulses. The pulses from each beamline can be spaced arbitrarily in time from 3 nsec to ≈ 100 μ sec. Such a Laser Radiographic Facility (LRF) would have substantial programmatic benefit beyond the radiographic application. With the addition of a second target chamber, equation of state measurements of unique materials could be conducted which cannot be conducted at Nova. In addition to EOS measurements, the 50 kJ at 1ω or ≈ 35 kJ at 3ω available from a 2x2 NIF style array would provide an ideal source for investigation of many other Stockpile related phenomena.

Laser Driven Radiography

Background

With the signing of the Comprehensive Test Ban Treaty, the Defense Programs Laboratories (LLNL, LANL and Sandia) are confronted with the challenge of certifying the safety and reliability of the United States nuclear stockpile without testing. To address this challenge the Laboratories and the Department of Energy have developed the Stockpile Stewardship and Management Program (SSMP). This program relies on scientific based assessment of the stockpile. This assessment is to be achieved by a variety of experimental and theoretical activities. The National Ignition Facility (NIF) and the ~~Advances~~ Strategic Computing Initiative (ASCI) are two pillars of this program. Another experimental facility designed to provide hydrodynamic data on macroscopic objects is the proposed Advanced Hydrodynamic Facility (AHF).

Currently, two technologies have been proposed to achieve time resolved, moderate resolution (≈ 1 mm) imaging to provide the hydrodynamic data necessary for realistic implosions. The first of these is a variation of the large scale induction accelerators which have been developed previously for this purpose at LLNL and LANL. These machines are linear induction devices capable of accelerating kiloamp currents to 15-20 MeV. These electrons strike a high atomic number target (e.g., Ta) producing copious hard x-rays from conventional Bremsstrahlung radiation. A conventional x-ray image is acquired of the object with a time resolution determined by the duration of the electron pulse (typically 50 nsec). Both LLNL and LANL have had single pulse, single axis machines of this type operational for over a decade. A single image of an imploding object is recorded on film similar to a conventional medical or industrial x-ray but at substantially higher photon energy. Unfortunately, these facilities do not provide the multi-axis, multiple pulse format required for tomographic reconstruction of an entire hydrodynamic experiment. A two axis facility, the Dual Axis, Hydrodynamic Radiographic Test Facility, DAHRT is under construction at Los Alamos. This facility will provide double pulse operation along two axes when it becomes operational in ≈ 2001 . These high energy flash x-ray sources have recently benefited from advances in solid-state switching technology and also from advances in x-ray recording media (intensified scintillator based detectors). The second technology which has been proposed for AHF is proton radiography. This approach requires a large scale, ≈ 1 GeV proton accelerator which provides imaging via energy loss in the target assembly.

Here, we propose a new concept for achieving high resolution, time resolved imaging of dense objects. In laser driven radiography, the essential idea is to utilize the x-rays produced when an intense laser pulse strikes a high Z target for conventional x-ray radiography. The use of laser plasmas as sources of x-rays for imaging small scale inertial confinement fusion targets has been performed for over a decade. As a result of the small scale of these targets and low ρr , relatively small amounts of low energy (2-10 keV) x-rays are required and easily achieved by utilizing as little as a few hundred joules of laser energy. The nanosecond duration of the x-ray burst and small source size are ideally suited to point source radiography in laser fusion. The requirements for large scale hydrodynamic experiments are orders of magnitude greater in both source strength and photon energy. Photon energies in the 2-10 MeV range and dose levels on the order of 100 Rads delivered 1 meter from the target are required. These requirements cannot be met by conventional laser sources. However, a new class of extremely high peak power lasers [1] offer the potential of laser matter interactions at an irradiance many orders of magnitude greater than achievable with even the most

advanced lasers employing conventional technology. These lasers are capable of producing petawatt (1000 TW) laser pulses and an irradiance approaching 10^{21} W/cm², far into the relativistic regime. In this regime the x-ray emission resulting from the interaction of petawatt class pulses with high Z targets is in the multi-MeV range.

The use of petawatt class lasers for the production of copious amounts of high energy x-rays has been discussed for over a decade.[2,3] In fact, intermediate energy (0.1-1 MeV) x-ray production with table-top size terawatt class lasers is now a sub-field within the strong-field interaction community. Numerous groups are developing or already using these small scale sources for radiography with bremsstrahlung spectra of a few hundred kilovolts.[4]

When an intense laser pulse strikes the target, electrons within the target are accelerated to relativistic velocities by the strong electric field ($\approx 10^{14}$ V/m). Some of these electrons are driven forward into the target (figure 1) producing a large current.

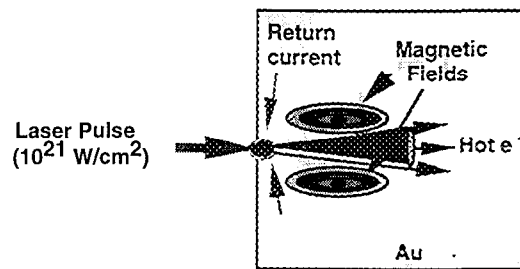


Figure 1: Schematic of laser produced Bremsstrahlung source.

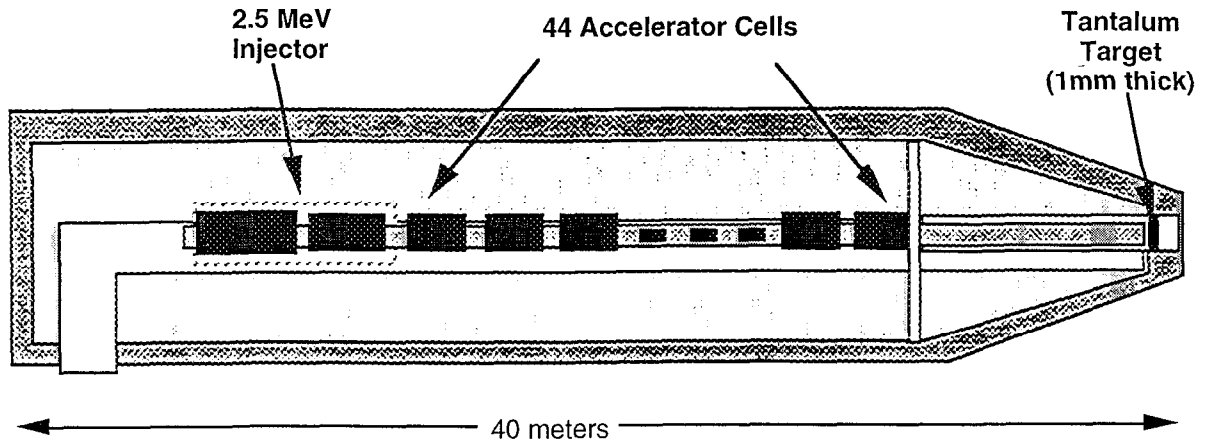
Although the details of this interaction are quite complex, the average electron energy in the hot plasma can be approximated by,

$$\langle E_e \rangle = m_e c^2 [1 + 2U_p / m_e c^2]^{1/2} \quad (1)$$

where U_p (eV) = $9.33 \times 10^{-14} I(\text{W/cm}^2) \lambda^2(\mu\text{m})$. This simple equation has been supported by numerous experiments and by detailed PIC simulations performed by Wilks [5] and others. Petawatt pulses focused to a few times the diffraction limit can achieve irradiances in excess of 1×10^{21} W/cm². At this irradiance, eq. 1 gives an average electron energy of 10 MeV. These hot electrons are produced in a forward directed "beam" in the target with a divergence determined by the incident intensity, target material (conductivity), magnetic fields generated, etc. These hot electrons will produce bremsstrahlung radiation in the target material similar to that produced from conventional electron accelerator sources.

While there is little doubt that petawatt lasers will produce a large amount of hard x-rays, the applicability of this source to radiographic applications of interest to Stockpile Stewardship is dictated by the absolute flux that can be produced in the 1-10 MeV range. In this regard, a comparison to existing accelerator sources is instructive. Essentially all large scale radiographic sources are based on LLNL induction accelerator technology. LLNL's Flash X-ray Facility (FXR, figure 2) produces a nominal current

of 2.2 kA in a 40 nsec pulse at an energy of 15 MeV. The electron spectrum of FXR is closely approximated by a narrow Gaussian distribution centered at 15 MeV. Of the 1300 J of electrons striking the target, only about 25% contribute to bremsstrahlung radiation within the solid angle defined by the ≈ 1 mm diameter collimator placed after the target.



LLNL Flash X-Ray (FXR) Facility

Injector Current	= 2.2 kA
Beam Energy	= 15 MeV
Pulse Duration	= 40 nsec
Pulse Energy	= 1320 J
Spot Size on Target	= 1.8 mm

Figure 2: Schematic of LLNL Flash X-ray Facility

The initial electron spectrum of an induction accelerator is quite different than the electron spectrum expected from the Petawatt at $1 \times 10^{21} \text{ W/cm}^2$. In figure 3, we display the initial electron spectrum from FXR and that predicted from the Petawatt interacting with a target of high conductivity. The Petawatt electron spectrum is estimated by

$$N(E)dE = C(E^{1/2}/\langle E_e \rangle^{3/2}) \text{Exp} [-E/\langle E_e \rangle] dE \quad (2)$$

where C is the normalization constant. This form of distribution has been shown to fit the electron spectra produced by the 100 TW laser with a high degree of accuracy and is supported by detailed PIC calculations[5].

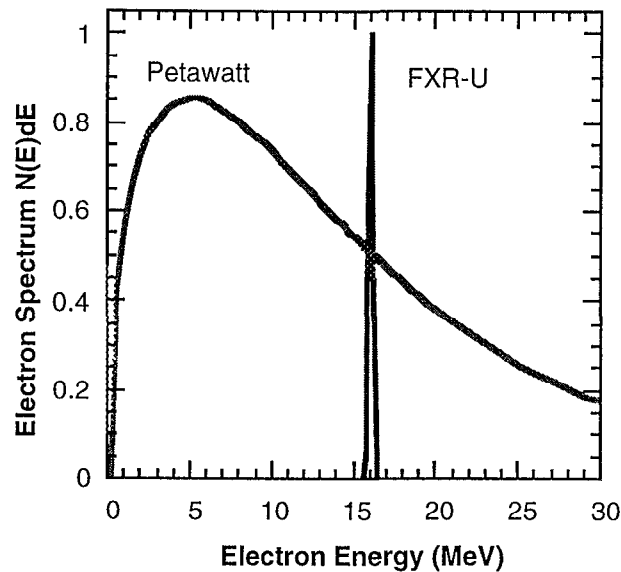


Figure 3: Electron spectra from FXR operating at 16 MeV and that predicted from the Petawatt at $1 \times 10^{21} \text{ W/cm}^2$.

While the initial electron spectra are quite different, the thin target Bremstrahlung spectra are surprisingly similar. These spectra, shown in figure 4, are obtained from the fully relativistic Schiff expression for the Bremstrahlung cross section [6,7]. Specifically, the differential cross section is integrated over the electron source distribution shown in figure 3. The strong differences between the initial electron distributions of the accelerator (nearly monoenergetic) and Petawatt (Maxwellian) are much less evident in the Bremstrahlung spectrum. This is a direct result of the energy and angular dependence of the Bremstrahlung cross section. Even a delta function electron distribution produces a broad x-ray spectrum.

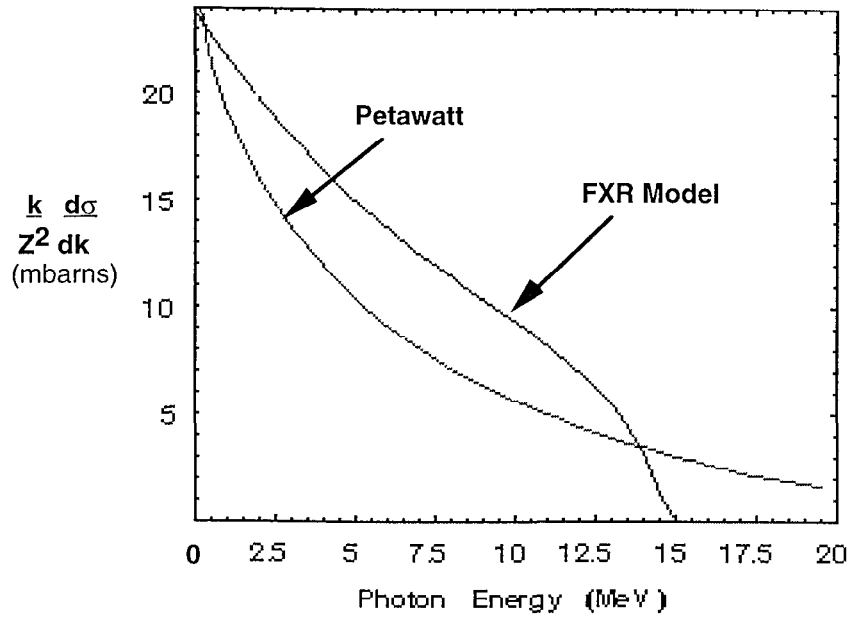


Figure 4: Thin target Bremsstrahlung spectrum for the FXR (blue) and Petawatt (red) source distributions shown in figure 3 (FXR operated $E_0=15$ MeV).

The differences between the two sources are even less evident when one considers the actual target used to tailor the x-ray spectrum. A typical FXR target consists of a thick radiator, (1 mm of Ta) followed by multiple layers of filtering material.[8] The x-ray spectrum produced by this target was modeled by using the thick target corrections suggested by Hisdal [6] and refined by Koch and Motz [7]. The thick target spectra were then multiplied by the transmission functions of the filter material to produce the spectra shown in Figure 5. In this figure, we present a comparison of the x-ray spectra from 1) our FXR model, 2) the “actual” FXR spectra provided by Norm Back, and 3) calculated for the Petawatt using the initial electron distribution shown in figure 2 and the filtered target assembly employed by the FXR (except for Au as the laser target). The use of a gold radiator instead of a tantalum radiator in the case of the Petawatt is dictated by the need for a material of high electrical conductivity (Conductivity: Gold= 4.55×10^5 (ohm-cm) $^{-1}$, Tantalum= 0.76×10^5 (ohm-cm) $^{-1}$, Copper = 5.88×10^5 (ohm-cm) $^{-1}$, Uranium= 0.39×10^5 (ohm-cm) $^{-1}$).

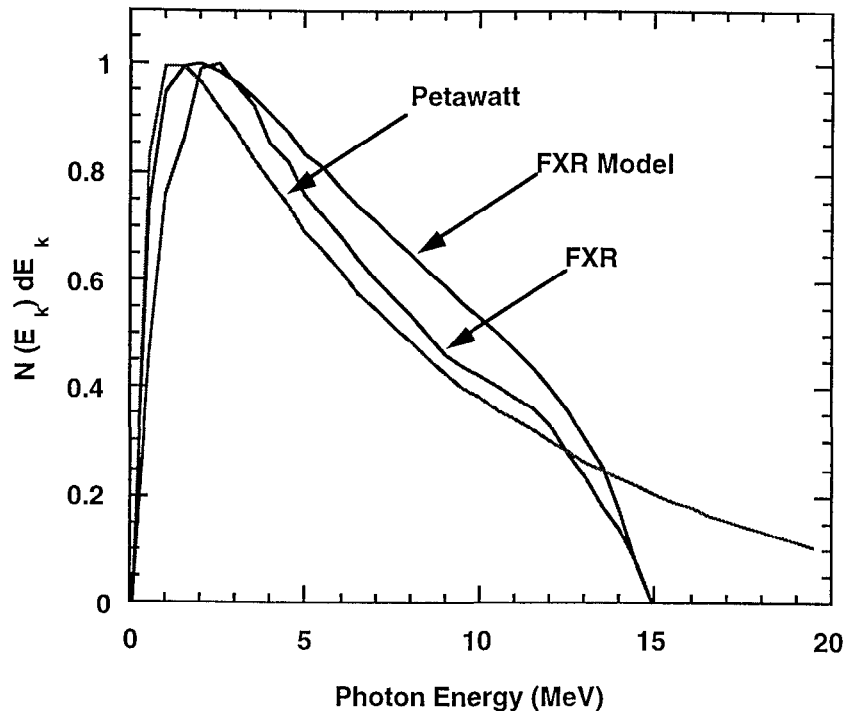


Figure 5: Estimated x-ray spectrum expected from the Petawatt at $1 \times 10^{21} \text{ W/cm}^2$ (blue), calculated FXR spectrum (red) and actual FXR spectrum (black).

Although the difference in the initial electron distributions of the induction accelerator and Petawatt source is large, the filtered bremsstrahlung spectra are quite similar. There is a slightly larger low energy component in both the estimated FXR and Petawatt spectra than is present in the actual FXR spectrum. The high energy tail in the Petawatt spectrum is a result of the high energy tail of the initial electron distribution.

Since the spectra produced by the two sources are similar, the efficacy of a laser produced hard x-ray source will be determined by the flux necessary to produce the desired radiograph. Utilizing new intensified detectors, high quality radiographs through the required μr are obtainable at 50 Rads with the FXR. Specifically, 50 Rads measured on axis at 1 meter from the tantalum target. It should be noted that FXR can produce ≈ 300 Rads at 1 meter. This dose is obtained with the collimator limiting the source size to ≈ 1 mm, i.e., the effective source is ≈ 350 J of 15 MeV electrons (1.5×10^{14} electrons) in a 1 mm diameter spot.

Calculations of the conversion efficiency from laser energy to hot electrons (>1 MeV) at $1 \times 10^{21} \text{ W/cm}^2$ vary from a low of 10% to a high of 80% [9]. Current experiments by Wharton, et al [10] using the LLNL 100 TW laser at $2 \times 10^{19} \text{ W/cm}^2$ yield conversion efficiencies of $\approx 25\%$ and experiments by Nickles [11], et al suggest conversion efficiency as high as 50% into hot electrons. Currently, the Petawatt can place 600 J on target and will be upgraded to 1 kJ by the end of December, 1997. The Petawatt can easily be run with three consecutive pulses separated by 10 nsec. With the current metallic compression gratings on the Petawatt, each pulse is limited to 1 kJ but a total of 3 kJ could be extracted for x-ray production in three separate pulses (1 kJ each). By using fused silica transmission gratings, individual Petawatt pulses with an energy as high as 5 kJ could be obtained. Using a conversion efficiency of 30%, suggests as much as 1.5 kJ of hot electrons could be produced per pulse.

Initial Experiments

To assess the potential for laser driven hard x-ray radiography we have begun an experimental campaign using Petawatt laser at LLNL. We present in this section a summary of the results of the first shot series.

Petawatt shots occurred during the week of September 5-10, 1997. Basic laser data was a pulse duration of 460 ± 40 fsec and a compressor throughput of 84%. Typical laser energy measured before compression was 450 J in a 46.3 cm diameter beam. Due to the hole in the paraboloid, 7.4% of the incident energy is lost. The beam was focused using a Cassegrainian telescope to a maximum irradiance of $\approx 10^{20}$ W/cm² on the best shots.

A typical target is shown in figure 6. The laser beam strikes the surface of the gold target at near normal (5°) incidence producing a strong relativistic electron current with a complicated angular distribution into the target. Electrons greater than approximately 2 MeV can escape the large space potential created within the target and penetrate the aluminum and CD₂ backing material. Electron spectrometers are placed in the plane of incidence at 30° from the laser axis and 95° from the axis. These electron spectrometers consist of a permanent dipole magnet with emulsion as the detector.

One way to examine the shot to shot performance is to plot the electron yield at 12.5 MeV and the photon yield above 1 MeV for each shot (figure 7). The first shot of the series, 27090507, produced the highest electron yield at 12.5 MeV and also exhibited the greatest asymmetry in the angular distribution of the electrons. A spectrum from this shot is shown in figure 3. Electrons were observed at energies extending above 90 MeV, however the bulk of the distribution was in the range of ~ 2 -15 MeV where the emission was found to be forward directed with about eight times more flux observed at 30° , with respect to the laser propagation direction, as compared to the flux at 95° . Note that an integration of the electron spectrum convolved with the bremsstrahlung cross section does not give an accurate estimate of the total photon yield or laser coupling efficiency since this electron spectrum is effected by the large space charge potential in the target and the energy loss (dE/dx) through the target assembly. The energy loss through the target for the electrons depicted in figure 8 was approximately 2.5 ± 0.5 MeV.

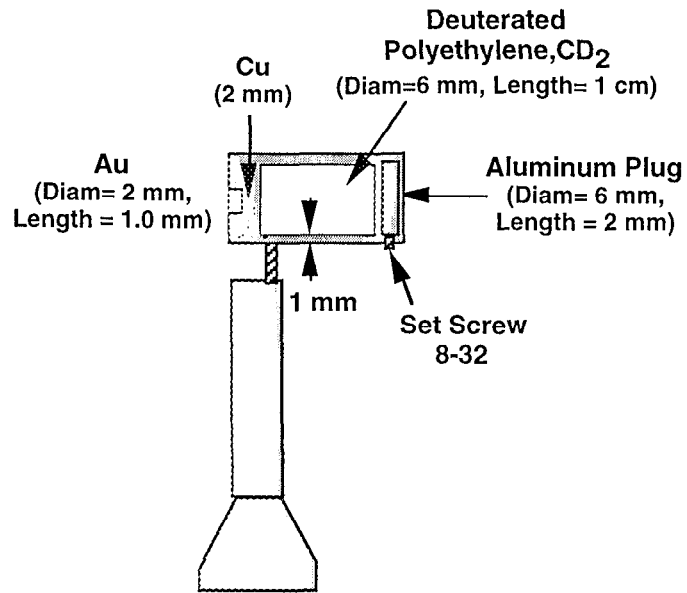


Figure 6: Petawatt radiography target

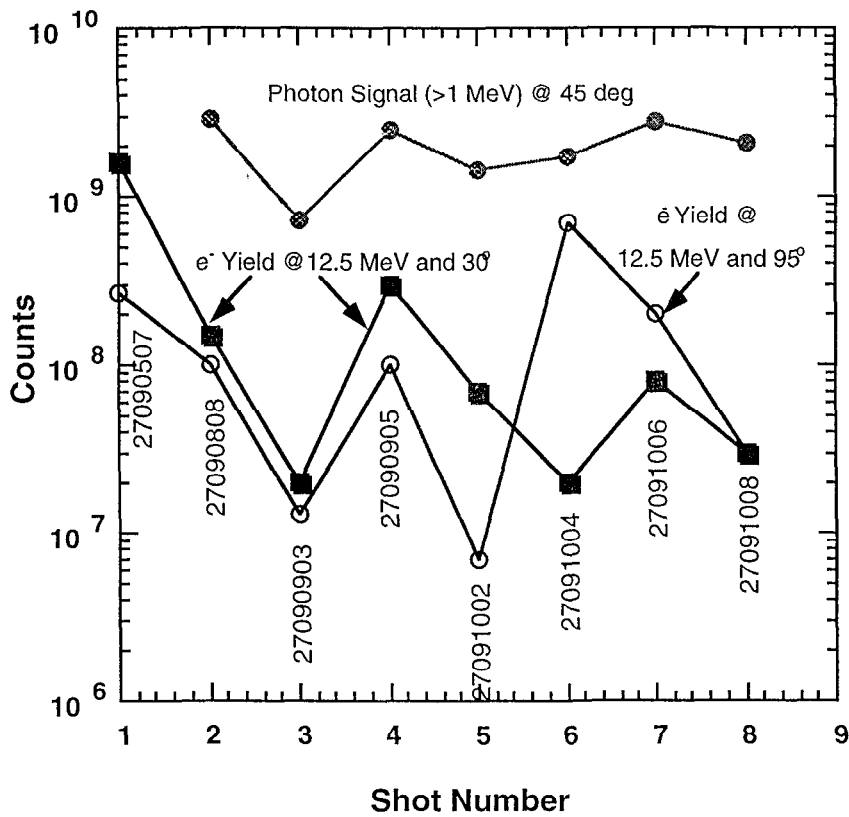


Figure 7: Variation of 12.5 MeV electron signal and $E_{\gamma} > 1$ MeV photons with shot number.

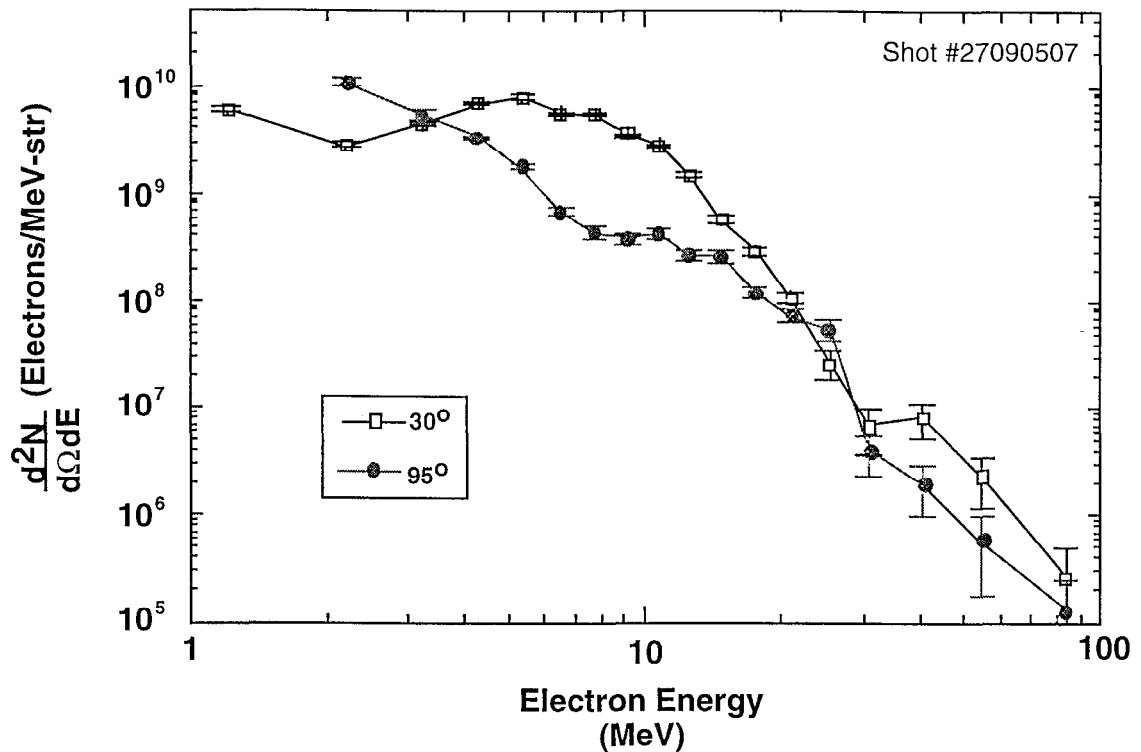


Figure 8: Electron spectra acquired at 30 and 95° with respect to the laser axis.

The space charge potential which is created within the target is a result of the short duration of the incident laser pulse. The electrons which are expelled from the target region create a deficit of charge which cannot be replenished within the 450 fsec duration of the laser pulse. For our conditions, numerical calculations suggest a space charge potential of approximately 1.5 MeV is established. This space charge potential represents a fundamental difference between short-pulse (<10 psec) interactions and more conventional laser-plasma interactions where substantial return current can be established during the laser pulse. Preliminary calculations suggest that these effects reduce the electron yield reaching the spectrometer by as much as 100 x. The data presented in figure 8 do not correct for these effects. The electron yield below approximately 5 MeV is unquestionably suppressed and the observed energy decreased from its initial value within the target. Aside from the suppressed region below ≈ 5 MeV, the electron spectrum can be well fit by a “two temperature” distribution. The spectrum observed at 30 degrees to the laser is shown in figure 9 along with two Maxwellian distributions given by eq. 2. The laser conditions for the spectrum depicted in figure 3 were such that $\approx 50\%$ of the 300 J incident on the target were focused within a $28 \times 40 \mu\text{m}$ spot. This corresponds to an average irradiance of $8 \times 10^{19} \text{ W/cm}^2$ for this shot. The average quiver energy for this irradiance (from eq. 1) is 2.95 MeV in remarkable agreement with the average electron energy characterizing the bulk of the distribution of figure 9.

The incident laser spot also contained sub-structure which would have seeded self-focusing in the preformed plasma. This self-focusing is almost certainly responsible for the “hot tail” of the distribution characterized by a second Maxwellian with an average electron energy of 11.5 MeV. This is consistent with PIC simulations which show the incident beam undergoing filamentation in the preformed plasma.

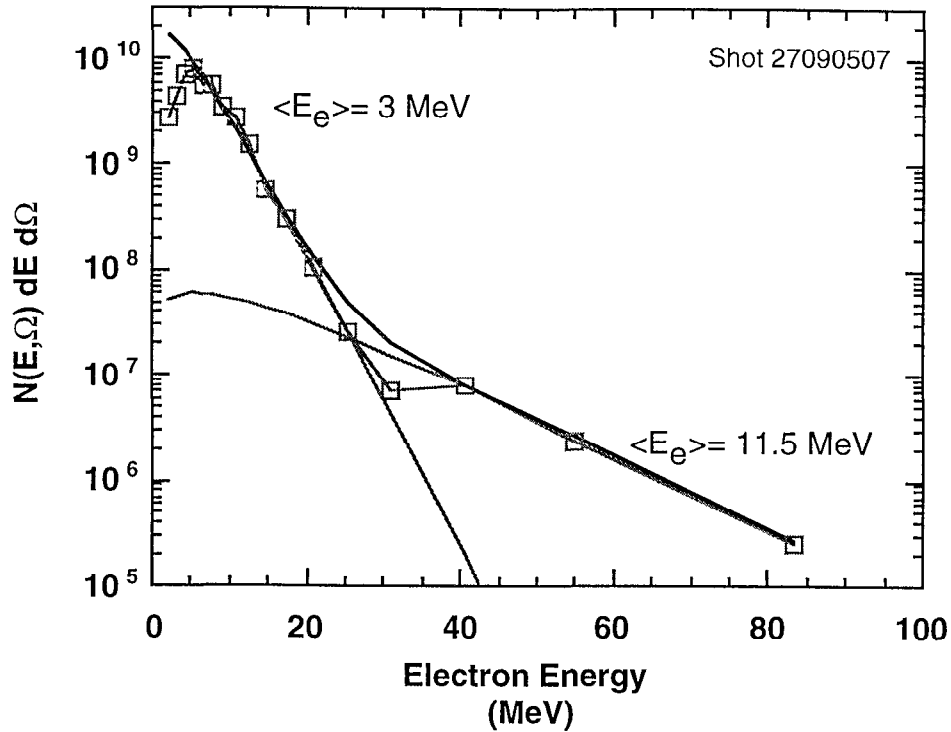


Figure 9: Electron Spectrum and calculated Maxwellian distributions (eq. 2)
The solid black curve is the sum of the two distributions.

High-energy bremsstrahlung x-rays generated by these electrons in the gold target will produce photonuclear reactions in almost all materials associated with the target assembly and vacuum chamber. The target itself was designed to measure the Bremsstrahlung spectrum by measuring the time of flight neutron energy spectrum associated with photodisintegration of deuterium, $D(\gamma,n)H$ [$Q=2.405 \text{ MeV}$]. The hard x-ray yield was so large however that the time of flight neutron scintillator array was overwhelmed by both prompt photons and background neutrons produced in the chamber walls.

Substantial radioactivity was measureable in the target assembly following the laser shot. This activity was due to photonuclear reactions in both the gold and surrounding copper target-holder producing transmutation to platinum and nickel daughter isotopes. The specific reactions observed include $^{197}\text{Au}(\gamma,n)^{196}\text{Au}$, identified by the decay of the ^{196}Au to ^{196}Pt emitting nuclear gamma-rays at 356 and 333 keV, and $^{63}\text{Cu}(\gamma,n)^{62}\text{Cu}$ and $^{65}\text{Cu}(\gamma,n)^{64}\text{Cu}$, which were identified by their subsequent beta decay (positron emission) to ^{62}Ni and ^{64}Ni (figure 10). Positron emission was determined by observation of 511 keV γ -rays resulting from annihilation radiation. Positive identification of both copper radioisotopes was established by fitting the decay curve with a two component decay with half-lives of 9.7 min and 12.7 hr (figure 10b). The fit gives an identification probability of better than 99% for ^{62}Cu and ^{64}Cu , respectively. The threshold gamma-ray energy for photo-activation of the gold is 8.06 MeV, ^{65}Cu is 9.91 MeV and 10.85 MeV for ^{63}Cu , indicating a large flux of high-energy bremsstrahlung.

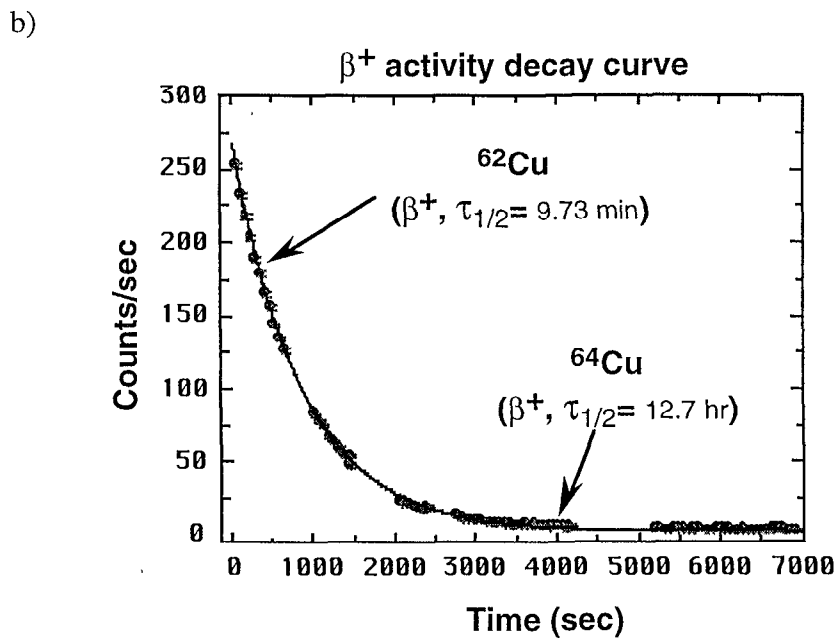
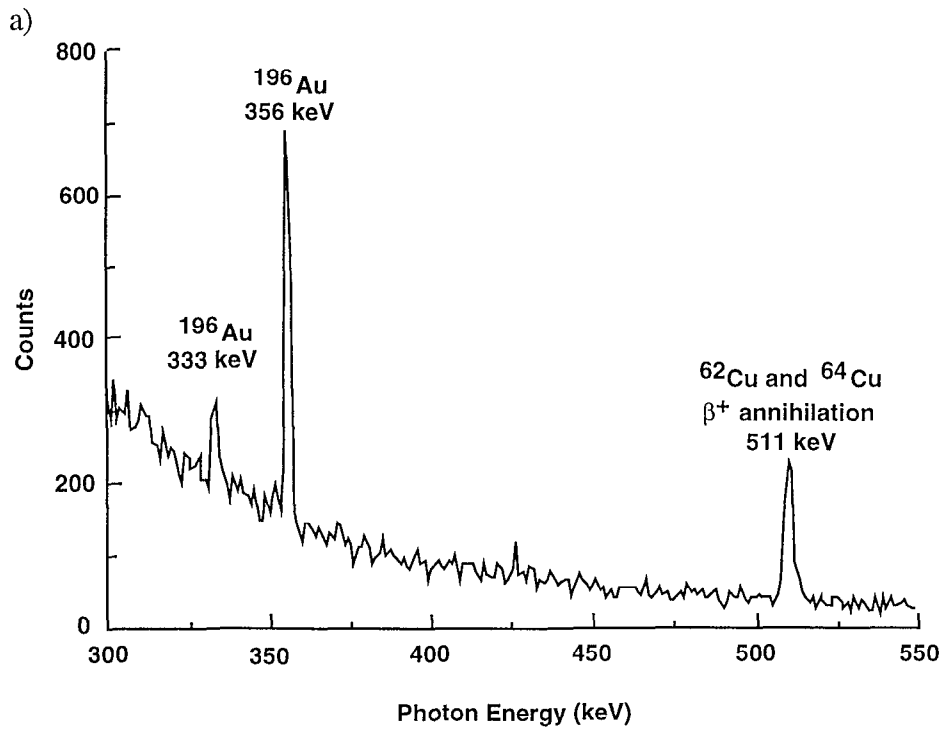


Figure 10: a) Gamma spectrum of target assembly acquired for ≈ 30 minutes. b) Decay curve of 511 keV annihilation peak with calculated decay curve for isotopic composition of natural copper.

Angular distribution measurements of the Bremsstrahlung yield were made by placing sodium iodide scintillators and PIN diodes at various locations around the chamber. These detectors were filtered by 1 inch lead such that they were sensitive to photons only above 1 MeV. The photon yield close to the laser axis ($\theta=5^\circ$) is consistently higher than the yield at 45° where most of the TLD data and radiographs are acquired. While there is insufficient data to provide an full measure of the angular distribution, the yield close to the laser axis is consistently a factor of 3 to 5 times larger than the photon yield measured at 45° .

Multiple radiographs thru varying thickness of lead were acquired during the shot series. Two of these, acquired with the film pack placed 81 cm from the target and at 45° to the laser axis, are shown in figures 11 and 12. The radiograph in figure 9 was acquired on shot 27090808 using tmh film. The depth designation on the figure corresponds to the amount of lead in front of the test object. For depth of 65, 80 and 108 mm, two additional features were machined into the object at 14 mm less depth of Pb. The radiograph in figure 12 is instructive since on these last two shots, high quality data was obtained from all diagnostics. The film pack was left in the target chamber for shots 27091004, 1006, and 1008. However, the x-ray yield from shot 27091004 was negligible relative to the other shots. Radiographs corresponding to a difference in film density of >0.2 can be observed thru 133 mm of lead ($\rho \approx 11.35 \text{ g/cm}^3$). Due to the attenuation of the lead, only photons with energy greater than approximately 1 MeV contributed to this radiograph. The integrated dose as measured from the TLDs at 100 cm from the target on these shots was: $0.1 < E_\gamma < 0.5 \text{ MeV} = 1.6 \times 10^9 \text{ photons/cm}^2$ (0.24 Rads), $0.5 < E_\gamma < 0.8 \text{ MeV} = 1.1 \times 10^8 \text{ photons/cm}^2$ (0.03 Rads), $0.8 < E_\gamma < 8 \text{ MeV} = 1.7 \times 10^8 \text{ photons/cm}^2$ (0.24 Rads) and $8 < E_\gamma < 20 \text{ MeV} = 5.5 \times 10^6 \text{ photons/cm}^2$ (≈ 0.02 Rads). The TLD spectrum is shown in figure 13.

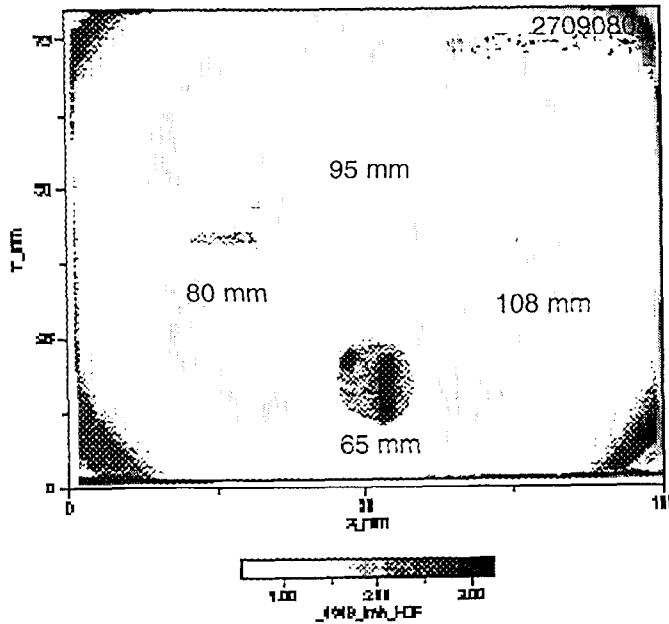


Figure 11: Radiograph acquired using tmh film at 45° to the laser axis through varying thickness of lead attenuator. The film pack was placed 81 cm from the target (Shot 2709080).

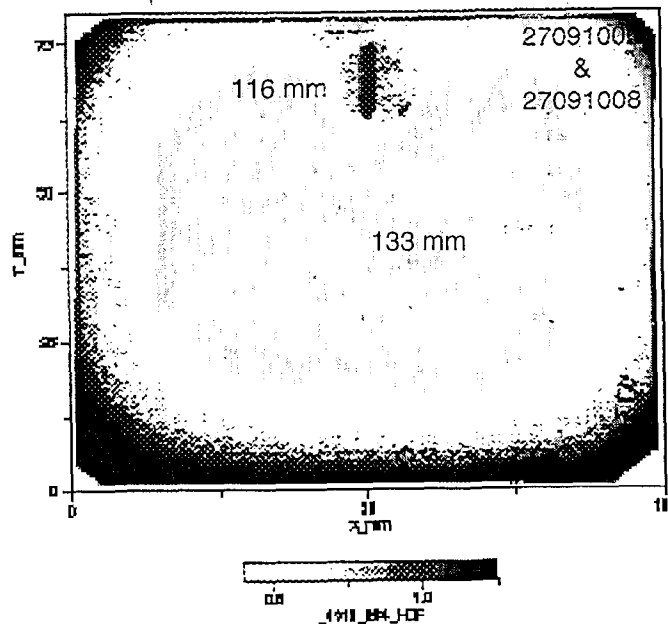


Figure 12: Radiograph acquired using bmx film at 45° to the laser axis through varying thickness of lead attenuator. The hard x-ray yield from two shots 27091006 and 1008 were summed together on this radiograph.

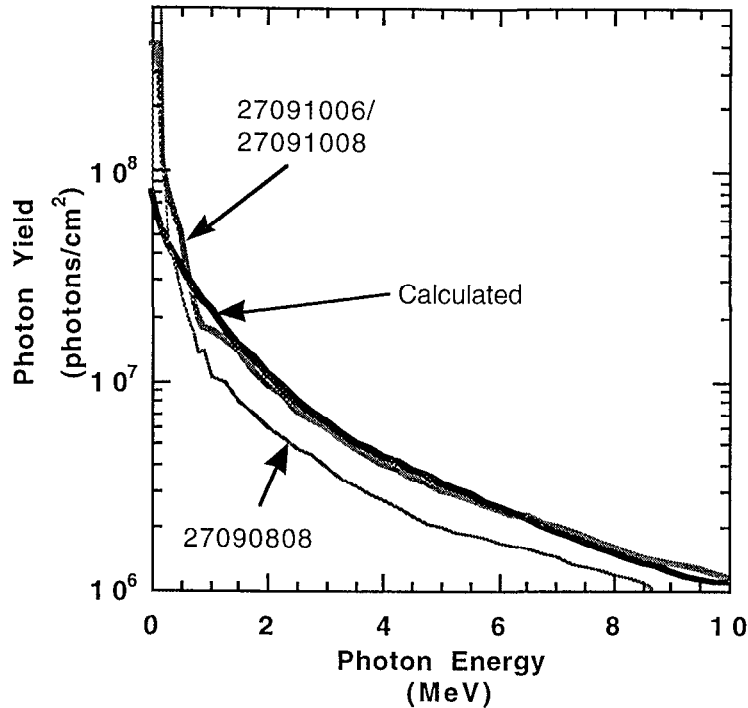


Figure 13: Bremsstrahlung spectra for various shots as acquired from thermoluminescent detectors placed 100 cm from the target at 45° to the laser axis.

High quality images of the far-field beam distribution were acquired on these shots (figure 14). The images show substantial beam distortion resulting from both pump-induced and thermal distortion in the Nova disk amplifiers. This distortion grows throughout the day as the amplifiers heat. Only 9.4 and 10% of the energy is contained within the central 25 μm spot, respectively for the two shots. The pulse energy was ≈ 280 and 290 J for the shots. As a result, in the absence of self-focusing, the highest irradiance present on target for these shots was $\approx 2 \times 10^{19}$ W/cm². Only the central spot would have had sufficient irradiance to produce hard (>1 MeV) x-ray photons. Hence, both the radiograph of figure 12 and the TLD spectrum of figure 13 were produced by ≈ 56 J (sum of energy within the central spot for 27091006 and 1008) focused to an irradiance of $\approx 2 \times 10^{19}$ W/cm².

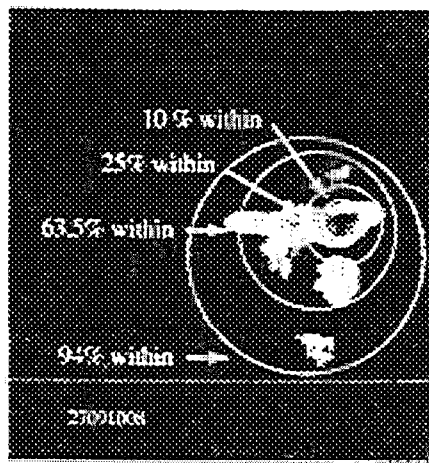
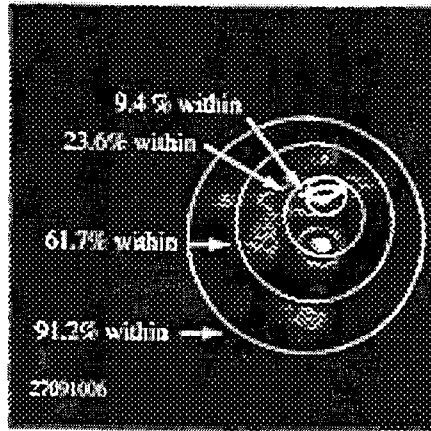


Figure 14: a) Far-field distribution from shot 27091006 and, b) shot 27091008.

The far-field distributions shown in figure 14 are the worst of the shot series (other than 27090903 which had the debris shield). In addition to serving as a testament to the need for the deformable mirror to correct this problem, the far-field data illustrates the need to account for the spatial distribution of irradiance in interpreting any shot data. The electron spectra are relatively insensitive to any portion of the distribution less than $\approx 10^{20}$ W/cm² since electrons below ≈ 3 MeV cannot escape the target as described previously. This is not the case of the Bremsstrahlung spectra which will include contributions from all hot electrons in the target. The thin target Bremsstrahlung spectra from the electron distributions of eq. 1 at 10^{19} W/cm² ($\langle E_e \rangle = 1$ MeV), $\approx 10^{20}$ W/cm² ($\langle E_e \rangle = 3$ MeV) and $\approx 10^{21}$ W/cm² ($\langle E_e \rangle = 10$ MeV) and a delta function distribution at $E_e = 10$ MeV are shown in figure 15. This figure dramatically illustrates the impact of beam quality on the Bremsstrahlung spectrum. A petawatt pulse focused to a 12 μ m diameter spot (10^{21} W/cm²) will produce more than 100 times the x-ray dose above 2 MeV as the same pulse focused to 10^{19} W/cm².

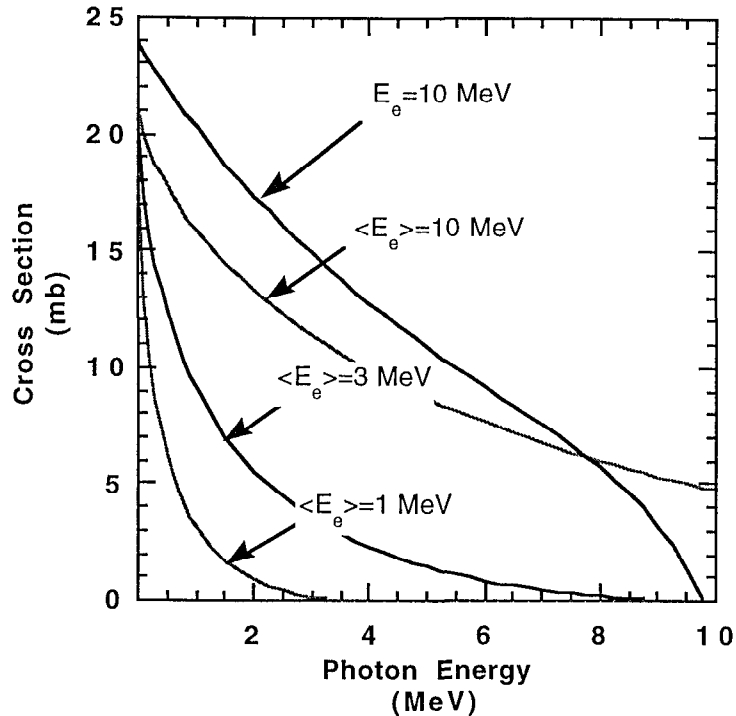


Figure 15: Thin target bremsstrahlung spectra for the electron distributions of eq. 1 and the characteristic energies shown. The upper most curve is the calculated spectrum for a monoenergetic 10 MeV electron beam.

The calculated spectrum in figure 13 is the result of calculating the bremsstrahlung spectra from the three distributions for $\langle E_e \rangle = 1$ MeV, $\langle E_e \rangle = 3$ MeV, and the same high energy tail as figure 9, $\langle E_e \rangle = 11.5$ MeV. The first two distributions were weighted approximately to the ratio of beam areas while the high energy distribution was weighted as necessary to fit the high energy tail. No attempt was made to fit the low energy ($E_\gamma < 0.2$ MeV) region of the spectrum since the data is unreliable here. Obviously there is a large low energy component due to the lower intensity regions of the laser pulse. Similar to the electron spectra in figure 9, there is a significant high energy component which is well described by a characteristic energy of ≈ 11.5 MeV. Presumably, this component is the result of self-focusing in the preformed plasma as described earlier. Note that the total number of high energy electrons produced by self-focusing is much less than the ratio indicated by fitting the bremsstrahlung spectrum due to the rapid scaling of the bremsstrahlung output with electron energy.

The total number of photons produced in the target above 0.8 MeV is $\approx 1.1 \times 10^{13}$ and above 8 MeV is $\approx 3.5 \times 10^{11}$ for the sum of shots 27091006 and 27091008. This is in good agreement with the number of radioactive gold nuclei produced by photoneutron emission. Integrating the photon spectrum above 8.06 MeV over the γ, n cross section ($\sigma_{\gamma, n} \approx 400$ mb at 10 MeV) for ^{197}Au yields $\approx 4 \times 10^8$ atoms of ^{196}Au should

have been produced in the target. The measured yield for these two shots was $2(\pm 1) \times 10^8$.

This laser produced hard photon source is an extremely intense source of MeV photons. Accounting for the source area, a photon fluence of $\approx 1.5 \times 10^{18}$ photons/cm² above 0.8 MeV was produced in the target. Since these photons are produced during the laser pulse only, the flux is on the order of 3.5×10^{30} photons/cm²-sec. This photon flux is large enough to exceed nuclear decay rates thereby enabling direct photoexcitation and even nonlinear optics (two photon absorption) in the gamma ray regime. In other words, this intense bremsstrahlung source acts for nuclear excitation analogous to an intense broadband thermal source (e.g., flashlamps) for atomic transitions.

In summary, the September shot series was highly successful in providing us our first data on this new type of source. High quality radiographs were obtained thru a > 150 g/cm² along with electron spectra extending to 100 MeV and photoactivation of the target assembly. The dose above ≈ 1 MeV measured using thermoluminescent detectors on the last two shots at 45° and 100 cm from the target was over 0.24 rads. Accounting for the difference in angular distribution (also measured on these shots), this would have corresponded to 0.6 ± 0.2 rads on axis. From the equivalent plane image, only 10% (56 J) of the incident laser energy was focused to a sufficient irradiance $\approx 2 \times 10^{19}$ W/cm² to have contributed to the dose above 1 MeV. As a result of the rapid scaling of the bremsstrahlung output with electron energy and hence laser irradiance, an increase in hard photon yield approaching two orders of magnitude may be achievable by improving the beam quality to enable an irradiance approaching 10^{21} W/cm² (800 J in 450 fsec focused to a 15 μ m diameter spot, 2x diffraction limited). These conclusions are supported by the large difference in the yield of high energy electrons from an early shot (27090507) with moderate beam quality ($> 1.6 \times 10^9$ e-/MeV-str) compared to that from a later shot with poor beam quality (27091006) 8.8×10^7 e-/MeV-str both at 30° and 12.5 MeV, a difference of 20. Finally, both in the electron and photon data, there is a strong high energy component which cannot be explained without filamentation of the beam in the preformed plasma resulting in small regions of locally high intensity or the presence of acceleration mechanisms.

We would like to acknowledge the help and advice of Dave Goosman, Norman Back.

References

1. M.D. Perry and G. Mourou, "Terawatt to Petawatt Class Lasers," *Science*, **264**, 917 (1994).
2. W. Friedhorsky, D. Lier, R. Day, and D. Gerke, "Hard x-ray measurements of 10.6 μm Laser Irradiated Targets," *Physical Review Letters*, **47**, 1661 (1981).
3. M.D. Perry, C. Keane, and E.M. Campbell, "Ultrahigh Brightness Lasers and their Applications," LLNL Internal document (1987).
4. J.D. Kmetec, C.L. Gordon, J.J. Macklin, B.E. Lemoff, and S.E. Harris, "MeV X-ray Generation with Femtosecond Lasers," *Physical Review Letters*, **68**, 1527 (1992).
5. S.C. Wilks, W. Kruer, M. Tabak, and A.B. Langdon, *Physical Review Letters*, **69**, 1383 (1992)
6. E. Hisdal, "Bremsstrahlung Spectra Corrected for Multiple Scattering in the Target," *Physical Review*, **103**, 1821 (1957).
7. H.W. Koch and J.W. Motz, "Bremsstrahlung Cross Section Formulas and Related Data," *Reviews of Modern Physics*, **31**, 920-955 (1959).
8. N. Back, "FXR Spectrum corrected for multiple scattering and filtering," June 1997.
9. P. Gibbon, "Efficient Production of Fast Electrons from Femtosecond Laser Interaction with solid targets," *Physical Review Letters*, **73**, 664 (1994).
10. K. Wharton, S.C. Wilks, S. Hatchett, et al, "Hot electron generation with intense femtosecond pulses," submitted to *Physical Review Letters*.

Technical Information Department • Lawrence Livermore National Laboratory
University of California • Livermore, California 94551

